

IMPACT: Behavioral Intention-aware Multimodal Trajectory Prediction with Addaptive Context Trimming

Jiawei Sun^{1*}, Xibin Yue², Jiahui Li¹, Tianle Shen¹, Chengran Yuan¹,
Shuo Sun¹, Sheng Guo¹, Quanyun Zhou², Marcelo H. Ang Jr¹
¹National University of Singapore ²Xiaomi EV

Abstract

While most prior research has focused on improving the precision of multimodal trajectory predictions, the explicit modeling of multimodal behavioral intentions (e.g., yielding, overtaking) remains relatively underexplored. This paper proposes a unified framework that jointly predicts both behavioral intentions and trajectories to enhance prediction accuracy, interpretability, and efficiency. Specifically, we employ a shared context encoder for both intention and trajectory predictions, thereby reducing structural redundancy and information loss. Moreover, we address the lack of ground-truth behavioral intention labels in mainstream datasets (Waymo, Argoverse) by auto-labeling these datasets, thus advancing the community's efforts in this direction. We further introduce a vectorized occupancy prediction module that infers the probability of each map polyline being occupied by the target vehicle's future trajectory. By leveraging these intention and occupancy predictions priors, our method conducts dynamic, modality-dependent pruning of irrelevant agents and map polylines in the decoding stage, effectively reducing computational overhead and mitigating noise from non-critical elements. Our approach ranks first among LiDAR-free methods on the Waymo Motion Dataset and achieves first place on the Waymo Interactive Prediction Dataset. Remarkably, even without model ensembling, our single-model framework improves the softmAP by 10% compared to the second-best method in Waymo Interactive Prediction Leaderboard. Furthermore, the proposed framework has been successfully deployed on real vehicles, demonstrating its practical effectiveness in real-world applications.

1. Introduction

In the realm of autonomous driving, accurately predicting the future behaviors of surrounding agents is crucial to ensure safe, efficient, and comfortable driving experience.

With mainstream approaches including [27, 36, 45,

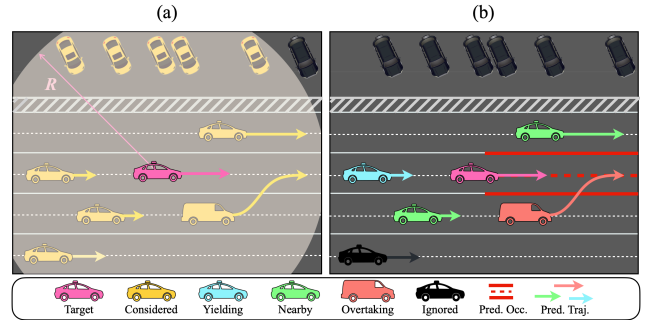


Figure 1. (a) illustrates the traditional predictor's context input, while (b) is our integrated approach jointly predicting behavioral intentions, trajectories, and vectorized occupancy. In our approach, the decoder stage is fed only with influential agents and relevant map elements.

[47] prioritising generating precise multimodal trajectory predictions, most recent research focused on achieving higher average precisions (mAP) and minimizing deviations (Brier-minFDE). However, humans primarily determine the future behavior of interacting agents not by focusing on specific states alone, but rather by inferring the underlying intention that drives their actions.

This insight is also applicable in autonomous driving, where predicting surrounding agents' future poses alone is insufficient and partial; understanding their behavioral intention (eg, yielding or overtaking) toward the ego vehicle is equally critical. Without explicit intention information, the downstream decision-making and planning modules are left with only a distribution of possible future coordinates. They must then infer the other vehicle's underlying behavior in an additional step, which not only complicates the ego vehicle's decision-making process but can also reduce the overall reliability and responsiveness of the system. The most straightforward method is to additionally incorporate one more behavioral intention prediction module, but this decoupled architecture inevitably introduces structural redundancy and information fragmentation.

Currently, most trajectory prediction models use attention mechanism for querying information from agents and

*This work was done during his internship at Xiaomi EV.

map features. However, indiscriminately attending to all agents and map elements introduces unnecessary complexity and potential causal confusion, as many elements have no direct relevance to the target agent, ultimately hindering correct decoding of the target agent’s future trajectories. To address this, some recent approaches introduce an additional local context-aware refinement module after the decoder stage [6, 43], but this further complicates the prediction pipeline. Others adopt rule-based heuristic pruning of input lanes [17] or dynamically collect map elements based on the previous layer prediction results [19, 26, 27, 29]. However, these methods may struggle in complex scenarios or suffer from error propagation. BETOP [20] is the first paper explicitly modelling agent interactions through braid theory, but its topological selection algorithm demonstrates critical accuracy deficiencies (see appendix). Thus, an efficient approach to selectively focus on truly critical features (both agents and maps) remains an open challenge. Furthermore, the lack of ground-truth intention labels in current mainstream datasets (e.g., Waymo [38], Argoverse [1, 2]) is limiting the development of accurate behavioral intention-aware models.

To holistically address the aforementioned challenges, we propose our approach, IMPACT. Specifically, we introduce an agent-wise multimodal behavioral intention module before the trajectory decoder, while sharing the same scenario information extraction module (i.e., the same encoder) used by the trajectory predictor. This design reduces computational overhead and mitigates information loss. The agent-wise behavioral intention module outputs a one-hot intention vector for each vehicle, where each element in the vector represents the probability of a specific intention relative to the ego vehicle (e.g., overtaking, yielding). Based on these probability vectors, we apply a utility function to assign an “interaction score” to each vehicle, selecting only those with high interaction probabilities as inputs to the decoder. In parallel, we propose a vectorized occupancy prediction module. This module predicts the probability that each vectorized map element will be occupied by the ego vehicle in the future. Similar to the agent selection process, we only feed the map polylines with high occupancy probabilities into the decoder. By integrating both modules in this manner, our method effectively reduces redundant interactions while preserving crucial information for accurate and robust trajectory prediction. We also propose an automatic labeling algorithm to generate high-quality ground truth labels for behavioral intentions on the Waymo and Argoverse 1&2 dataset.

We evaluated IMPACT on both the Waymo Motion Prediction Dataset (for marginal prediction) and the Waymo Interactive Prediction Dataset (for interaction prediction). Experimental results demonstrate that our method achieves the best performance among all LiDAR-free methods on

the Waymo Motion Prediction Dataset, surpassed only by MTRV3 [25], which leverages additional LiDAR data. Moreover, IMPACT ranks first overall on the Waymo Interactive Prediction Dataset, surpassing the previous state-of-the-art ensemble model [20] using only a single model. To further demonstrate the practical applicability of our approach, we successfully trained IMPACT on a proprietary dataset and deployed it effectively on a real vehicle.

Our main contributions can be summarized as follows:

1) **Intent-Integrated Trajectory Prediction.** We jointly predict agent multimodal intentions and trajectories in a unified framework, eliminating redundant modules and enhancing information flow.

2) **Context-Aware Pruning via Dual Filters.** We introduce complementary agent and map filters that leverage predicted behavioral interaction probabilities and vectorized occupancy to retain only influential vehicles and relevant map elements.

3) **Automatic Intention Label Generation.** We propose an automatic labeling strategy to annotate agent-level intentions in large-scale datasets (e.g., Waymo, Argoverse). This strategy enables more convenient behavior prediction without manual effort.

4) **State-of-the-Art Performance and Real-World Validation.** IMPACT achieves SOTA results on mainstream public benchmarks and demonstrates robust real-world performance through deployment on an autonomous vehicle (a video demo in supplementary material).

2. Related Works

2.1. Motion Prediction

Early approaches [4, 12, 24] relied on Bird’s-Eye-View (BEV) rasterized representations processed through CNNs, but struggled to preserve geometric fidelity and semantic relationships. This limitation spurred vectorized paradigms like VectorNet [11], which encoded agents and map elements as polylines. Subsequent graph-based architectures [7, 15] further formalized relational dependencies through graph neural networks. The field then diverged into anchor-oriented strategies [13, 33, 41, 43] leveraging HD map anchors for physically constrained prediction, followed by agent-centric frameworks [26, 44]. But it requires re-normalizing and re-encoding during online inference. Query-centric approaches [27, 35, 40, 45, 46] addressed this by encoding each vehicle as a query, leveraging attention mechanisms to enhance prediction performance and improve multi-agent coherence through unified spatio-temporal encoding. Recent research in motion forecasting has witnessed significant advancements across multiple frontiers, driving improvements in generalization, consistency, and predictive accuracy. Self-supervised ap-

proaches [3, 5, 17] enhance model generalization by leveraging reconstruction pretext tasks, while temporal consistency methods [28, 32, 39] reinforce scene coherence through continuous-time modeling. At the same time, architectures like RMP-YOLO [29, 37] tackle the challenge of partial observations by imputing missing trajectory segments. Furthermore, ModeSeq [47] introduces a paradigm shift by framing motion prediction as a GPT-style next-token prediction task.

However, current methods tend to emphasize the precise generation of multimodal trajectory predictions at the expense of behavioral intention prediction [8] (BIP). This narrow focus often overlooks the latent decision-making processes that drive observable maneuvers, resulting in models that struggle to interpret complex social interactions or anticipate nuanced changes in driving behavior. In real-world scenarios, the inability to infer intentions such as overtake or yield decisions can lead to suboptimal planning and reduced overall robustness. The most recent work, BeTOP [20], attempts to explicitly model behavioral interactions via braid theory by splitting agents into “interactive” and “non-interactive” based on whether their future trajectories form an intertwined braid. However, in most scenarios (see Appendix), the generated braids appear unrealistic because the approach only considers lateral and temporal dimensions. Moreover, relying on a binary behavioral label oversimplifies complex traffic scenarios, where interactions can be far more nuanced.

Our IMPACT framework addresses these limitations by jointly predicting multimodal, multi-class behavioral intentions and future trajectories. To better supervise the behavioral intention predictor, we propose an auto-labeling algorithm that generates reasonable intention labels, striking a balance between explainability and behavioral completeness.

2.2. Context-aware Pruning

During the decoder stage, current works often relies on attention mechanisms [34] to query agent-map information. However, using global attention over all entities incurs $O(n^2)$ complexity and can introduce causal confusion, in contrast to human drivers, who primarily focus on goal-critical paths and potentially interactive vehicles [8]. Some approaches address this via prior rule-based pruning (e.g., SEPT [17]), which may fail for corner case. Meanwhile, MTR-series [10, 18, 22, 26, 27, 29, 30, 42] methods and R-pred [6] use last layer predictions as priors to dynamically collect nearby polylines, yet suffers from error propagation. BeTOP [20], which relies on braid theory to select interactive vehicles, can yield an unreasonably chosen set of vehicles in practice. To tackle these issues, our IMPACT framework introduces a symmetric dual context-filtering approach that leverage predicted behavioral inter-

action probabilities and vectorized occupancy to retain only influential vehicles and relevant map elements.

3. Methodologies

3.1. Problem Formulation

Following the vectorized representation in VectorNet, we denote the historical trajectories of N_a traffic participants as $\mathcal{A} = \{a_1, a_2, \dots, a_{N_a}\}$. The corresponding map is equally partitioned into N_l polylines $\mathcal{L} = \{l_1, l_2, \dots, l_{N_l}\}$. The predictor will anticipate K different modality future trajectories $\mathcal{Y} = \{y_1, y_2, \dots, y_{N_a}\}$ over the future T_f timesteps, where $y_i = \{y_i^1, y_i^2, \dots, y_i^K\} \in \mathbb{R}^{K \times T_f \times 2}$. The confidence score for y_i are denoted as $s_i = \{s_i^1, s_i^2, \dots, s_i^K\}$. Then for target agent a_i , existing motion prediction task aims to estimate the distribution:

$$P(y_i | \mathcal{L}, \mathcal{A}) = \sum_{k=1}^K s_i^k P(y_i^k | \mathcal{L}, \mathcal{A}) \quad (1)$$

To better capture inter-agent interactions and crucial map segments, we additionally predict two sets of modality-dependent priors: behavioral intentions $\mathcal{H}^k = \{h_1^k, \dots, h_{N_a}^k\}$, where $h_i^k \in \mathbb{R}^4$ encodes the probability distribution of behavioral intentions (overtaking, yielding, ignored, nearby) for agent a_i toward target agent under mode k and vectorized occupancy $\mathcal{O}^k = \{o_1^k, \dots, o_{N_l}^k\}$, where $o_j^k \in [0, 1]$ indicates the probability that polyline l_j is relevant or “occupied” by the agent’s future path under mode k . Given $\{\mathcal{H}^k\}$ and $\{\mathcal{O}^k\}$, we perform a top- m selection of agents and top- n selection of map polylines for each modality k :

$$\begin{aligned} \mathcal{A}_k^{\text{sel}} &= \{a_j : j \in \text{argtop}_m[\psi(h_j^k)]_{j=1}^{N_a}\}, \\ \mathcal{L}_k^{\text{sel}} &= \{l_j : j \in \text{argtop}_n[\varphi(o_j^k)]_{j=1}^{N_l}\}. \end{aligned} \quad (2)$$

where $\psi(h_j^k)$ and $\varphi(o_j^k)$ is a scalar score derived from the intention vector h_j^k and occupancy vector o_j^k by utility function $\psi(\cdot)$ and $\varphi(\cdot)$. These subsets ensure that each modality k focuses only on the most critical agents and polylines.

To jointly capture both the behavioral intentions and the map occupancy, we consider the extended distribution:

$$P(y_i, \mathcal{H}, \mathcal{O} | \mathcal{L}, \mathcal{A}) \approx \sum_{k=1}^K s_i^k P(\mathcal{H}^k | \mathcal{L}, \mathcal{A}) P(\mathcal{O}^k | \mathcal{L}, \mathcal{A}) P(y_i^k | \mathcal{A}_k^{\text{sel}}, \mathcal{L}_k^{\text{sel}}). \quad (3)$$

Where $P(\mathcal{H}^k | \mathcal{L}, \mathcal{A})$ yields the intention vectors for each agent under mode k , $P(\mathcal{O}^k | \mathcal{L}, \mathcal{A})$ produces occupancy scores for each polyline under mode k , $\mathcal{A}_k^{\text{sel}}$ and $\mathcal{L}_k^{\text{sel}}$ are the selected agents/polylines for each modality, and the final trajectory y_i^k is decoded by attending only to these subsets. This operation reduces cross-attention complexity from $O(KN_a + KN_l)$ to $O(Km + Kn)$ while maintaining accuracy.

3.2. Input Representation

In our method, we apply agent-centric normalization. To predict a target agent, the input to the predictor comprises:

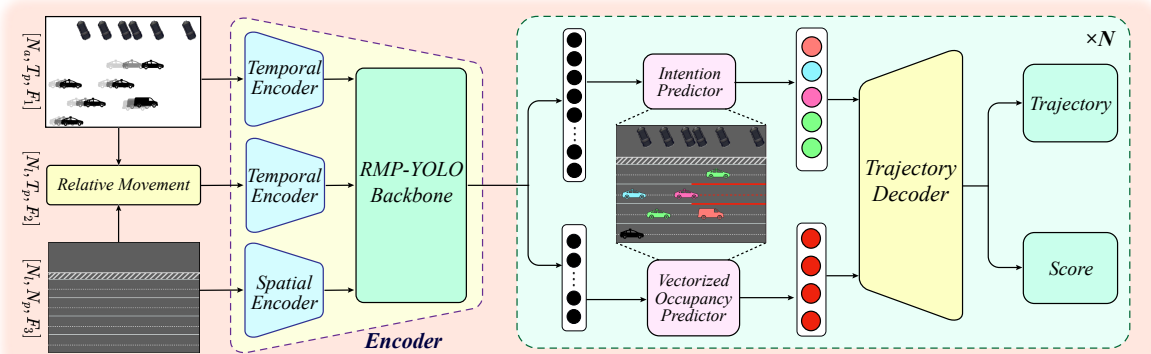


Figure 2. An overview of framework of IMPACT. Both the Intention Predictor and the Vectorized Occupancy Predictor share the same context encoder with the Trajectory Decoder, leveraging their outputs to prune irrelevant agents and map polylines. This selective mechanism ensures that only the most critical context is fed into the decoder for final trajectory prediction.

$A = \{a_1, a_2, \dots, a_{N_a}\} \in \mathbb{R}^{N_a \times T_p \times F_1}$, representing N_a agents with T_p past states and feature dimension F_1 , and $\mathcal{L} = \{l_1, l_2, \dots, l_{N_l}\} \in \mathbb{R}^{N_l \times N_p \times F_2}$, representing N_l polylines with N_p points each and feature dimension F_2 .

Following the approaches of RMP-YOLO[29] and MacFormer[9], we further incorporate the historical relative movement between the target agent and the map polylines to capture dynamic subtle interdependencies. This historical movement is denoted by $\mathcal{R} = \{r_1, r_2, \dots, r_{N_l}\} \in \mathbb{R}^{N_l \times T_p \times F_3}$, where F_3 is the feature size associated with the relative movement $((\Delta x, \Delta y, \cos \Delta \theta, \sin \Delta \theta))$.

3.3. Network Structure

3.3.1. Spatial Temporal Encoding

To comprehensively model temporal dependencies, we apply a Multi-Scale LSTM (MSL) module. The time-series data \mathcal{A} and \mathcal{R} are each processed through three parallel streams. Each stream consists of a 1D CNN with a distinct kernel size followed by an LSTM. For the i -th stream with kernel size k_i , the output at the final time step T_p is computed as:

$$\mathcal{A}_{k_i}^{T_p} = \text{LSTM}(\text{Conv1D}_{k_i}(\mathcal{A})) \Big|_{t=T_p}, \quad k_i \in \{1, 3, 5\} \quad (4)$$

$$\mathcal{R}_{k_i}^{T_p} = \text{LSTM}(\text{Conv1D}_{k_i}(\mathcal{R})) \Big|_{t=T_p}, \quad k_i \in \{1, 3, 5\} \quad (5)$$

The final-step hidden states are concatenated (\oplus) along the feature dimension, and a multi-layer perceptron (MLP) projects the concatenated vector into a unified temporal feature token:

$$\mathcal{A}^1 = \text{MLP}(\mathcal{A}_1^{T_p} \oplus \mathcal{A}_3^{T_p} \oplus \mathcal{A}_5^{T_p}) \in \mathbb{R}^{N_a \times D}, \quad (6)$$

$$\mathcal{R}^1 = \text{MLP}(\mathcal{R}_1^{T_p} \oplus \mathcal{R}_3^{T_p} \oplus \mathcal{R}_5^{T_p}) \in \mathbb{R}^{N_l \times D}. \quad (7)$$

For the spatial data \mathcal{L} , we adopt a simplified PointNet-like architecture to aggregate each polyline into a feature token:

$$\mathcal{L}_1 = \text{MaxPooling}(\text{MLP}(\mathcal{L})) \in \mathbb{R}^{N_l \times D}. \quad (8)$$

These tokens are aligned in the feature space (\mathbb{R}^D) and ready for downstream fusion and prediction tasks.

3.3.2. Feature Fusion.

We utilize RMP-YOLO's encoder[29] as a backbone network (see Figure 2) to do feature fusion. To integrate heterogeneous input modalities, we employ a cascaded Multi-Context Gating (MCG) mechanism inspired by [33]. The MCG modules sequentially fuse pairs of modalities from a candidate set of three. The output of each MCG stage serves as input to the subsequent stage, enabling hierarchical feature interaction:

$$(\mathcal{A}^2, \mathcal{R}^2) = \text{MCG}(\mathcal{A}^1, \mathcal{R}^1), \quad (9)$$

$$(\mathcal{L}^2, \mathcal{R}^3) = \text{MCG}(\mathcal{L}^1, \mathcal{R}^2), \quad (10)$$

$$(\mathcal{A}^3, \mathcal{L}^3) = \text{MCG}(\mathcal{A}^2, \mathcal{L}^2), \quad (11)$$

The final fused tokens are defined as agent tokens: $\mathcal{A}_3 \in \mathbb{R}^{N_a \times D}$ and map tokens: $\mathcal{L}_3 = \mathcal{L}_3 + \mathcal{R}_3 \in \mathbb{R}^{N_p \times D}$. Thus, we design a K-nearest-neighbor (KNN) guided local attention mechanism to restrict each agent token to attend only to its K most relevant neighboring tokens (agents or map elements). This sparse attention pattern reduces computational complexity while preserving critical interactions. Six transformer encoder layers are applied to achieve deep feature fusion. Each layer follows the standard transformer architecture enhanced with positional encoding:

$$X^i = \text{MHA}(X^{i-1} + \text{PE}(X^{i-1}), \mathcal{K}(X^{i-1}) + \text{PE}(\mathcal{K}(X^{i-1})), \mathcal{K}(X^{i-1})) \quad (12)$$

where $X^0 = [\mathcal{L}_3, \mathcal{A}_3] \in \mathbb{R}^{(N_a + N_m) \times D}$, $\text{MHA}(\cdot)$ denotes multi-head attention, $\mathcal{K}(\cdot)$ selects K -nearest neighbors via Euclidean distance, and $\text{PE}(\cdot)$ injects positional information using sinusoidal encoding. The positional coordinates derive from agents' latest observed positions and map polylines' centroid coordinates. The final output tokens $X^{\text{final}} = [\mathcal{L}_4, \mathcal{A}_4]$ are fed into the behavioral intention prediction module and vectorized occupation prediction for dynamic context-aware pruning.

Before diving into decoder part (see Figure 3), we define query content feature at decoder layer i as $Q^i \in \mathbb{R}^{K \times D}$, which are later used to aggregate information from agent tokens and map tokens, and decode multimodal prediction results and K denotes the number of different futures.

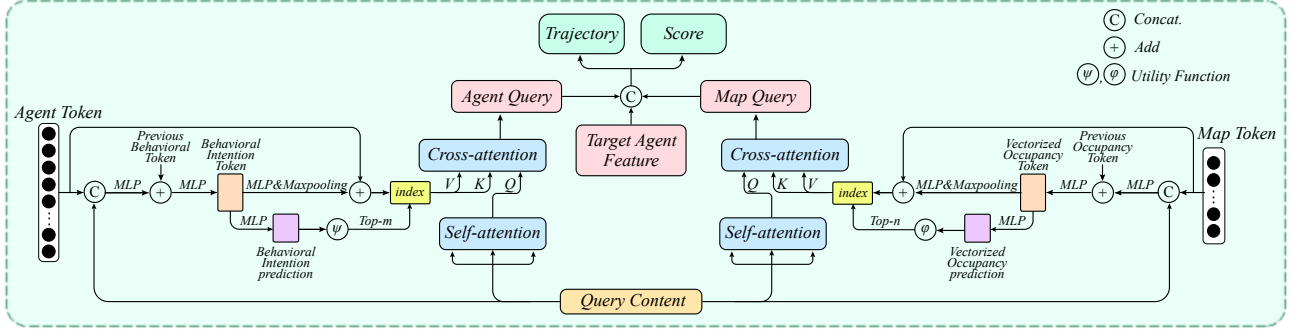


Figure 3. An overview of our decoder framework, featuring context-aware pruning via symmetric dual filters.

3.3.3. Multimodal Behavioral Intention Prediction

For each future modality, we predict the behavioral intentions of other agents with respect to the target agent. Given the input agent tokens $\mathcal{A}_4 \in \mathbb{R}^{N_a \times D}$ and the query content $Q^i \in \mathbb{R}^{K \times D}$, we fuse these features into a unified representation of shape $\mathbb{R}^{K \times N_a \times 2D}$ via straightforward tensor broadcasting and concatenation. Next, the fused features are passed through a multi-layer perceptron (MLP) and then added to the previous layer’s behavioral intention token $I^{i-1} \in \mathbb{R}^{K \times N_a \times D}$. Finally, another MLP followed by a softmax activation function produces the final behavioral intention predictions:

$$\begin{aligned} \hat{H}^i &= \text{Softmax}\left(\text{MLP}(I^i)\right) \in \mathbb{R}^{K \times N_a \times 4}, \\ I^i &= \text{MLP}(\text{MLP}(\mathcal{A}_4 \oplus Q^i) + I^{i-1}). \end{aligned} \quad (13)$$

Each vector element h represents a probability distribution over four intention categories: *yielding*, *overtaking*, *ignored*, and *nearby*. To make the decoding process more focused, we first compute an overall interaction score from the predicted distribution \hat{H} using a utility function ψ , producing $\psi(\hat{H}^i) \in \mathbb{R}^{K \times N_a}$. We then select the top- m highest-scoring agents for downstream trajectory decoding. Therefore, for each modality, we choose m most relevant agents $\mathcal{A}_5 \in \mathbb{R}^{m \times D}$, where $m \ll N_a$. This filtering step refines the decoder’s input, concentrating on the most influential interactions while improving prediction accuracy. The ground-truth label of behavioral intention H^* is derived from an auto-labeled data preprocessing process (see Appendix).

3.3.4. Multimodal Vectorized Occupancy Prediction

Unlike conventional occupancy prediction methods that rely on computationally intensive rasterization of multi-view images, we introduce a novel vectorized occupancy prediction framework that integrates seamlessly with our vectorized scenario representation. For each map polyline l_i , we predict multimodal occupancy probabilities corresponding to different future hypotheses of the target agent. Denoting C^{i-1} as the previous vectorized occupancy tokens, we apply an operation symmetric to the multimodal behavioral intention prediction:

$$\begin{aligned} \hat{O}^i &= \text{Sigmoid}\left(\text{MLP}(C^i)\right) \in \mathbb{R}^{K \times N_l \times 1}, \\ C^i &= \text{MLP}(\text{MLP}(L_4 \oplus Q^i) + C^{i-1}) \end{aligned} \quad (14)$$

This vectorized approach ensures both efficiency and scalability while maintaining alignment with the overall vectorized representation of the scene. Among the N_l polylines’s multimodal occupancy probabilities $\varphi(\hat{O}^i) \in \mathbb{R}^{K \times N_l}$, we select the top- n with the highest predicted probabilities in each modality to form $L_5 \in \mathbb{R}^{n \times D}$, where $n \ll N_l$. These top-ranked polylines serve as focused inputs for the subsequent trajectory decoder. The ground-truth occupancy label O^* is also derived from an auto-labeled data preprocessing process (see Appendix).

3.3.5. Trajectory Decoder

We adopt a multi-layer MTR-style[26] trajectory decoder. At each layer i , self-attention is applied to the query content $Q^i \in \mathbb{R}^{K \times D}$ across the K motion modes, enabling information exchange among different future modalities. Subsequently, for each modality, two cross-attention modules integrate features from the filtered agent tokens \mathcal{A}_5 and map tokens L_5 . Finally, the target agent feature (replicated K times) is concatenated with the cross-attended query features, and passed through a regression head to generate a set of Gaussian Mixture Model (GMM) parameters at each future timestep: $\left\{(\mu_x^k, \mu_y^k, \sigma_x^k, \sigma_y^k, \rho^k)\right\}_{k=1}^K$, where $(\mu_x^k, \mu_y^k, \sigma_x^k, \sigma_y^k, \rho^k)$ parameterizes the k -th Gaussian component. In addition, a classification head outputs the confidence scores $S \in \mathbb{R}^K$ corresponding to each motion mode. This multimodal representation captures the inherent uncertainties of agent trajectories.

3.4. Training Loss

Our overall training objective comprises four components:

$$\mathcal{L}_{\text{total}} = \lambda_1 \mathcal{L}_{\text{Int}} + \lambda_2 \mathcal{L}_{\text{Occ}} + \lambda_3 \mathcal{L}_{\text{Traj}} + \lambda_4 \mathcal{L}_{\text{Score}}, \quad (15)$$

where $\lambda_1, \lambda_2, \lambda_3$, and λ_4 are weighting factors balancing the contributions of behavioral intention prediction, vectorized occupancy prediction, trajectory prediction, and mode classification, respectively. Specifically, \mathcal{L}_{Int} is calculated using the multi-class Focal Loss, \mathcal{L}_{Occ} is based on the binary Focal Loss, $\mathcal{L}_{\text{Traj}}$ is derived from the GMM loss, and $\mathcal{L}_{\text{Score}}$ is computed with Binary Cross-Entropy. During training, the winner-take-all strategy is applied for \mathcal{L}_{Int} , \mathcal{L}_{Occ} , and $\mathcal{L}_{\text{Traj}}$, ensuring that only the modality closest to the ground-truth trajectory is used to compute these losses. Please check appendix for more details.

4. Experiments

4.1. Experimental Setup

Datasets and Evaluation Metrics. Our experiments are conducted on one of the most challenging prediction datasets, Waymo Open Motion Dataset (WOMD)[38]. This large-scale dataset comprises 486,995 training clips, 44,097 validation clips, and 44,920 testing clips. Each clip contains 10 timesteps of historical agent states, 1 current timestep, and 80 future timesteps at a sampling frequency of 10 Hz, along with HD map information. We evaluate our method on both core WOMD tasks: the marginal motion and interactive motion prediction tasks. Following the standard evaluation protocol, we adopt metrics including Soft mAP, mAP, minADE, minFDE, Miss Rate, and Overlap Rate, and Soft mAP is the main metric.

Implementation Details. We employ AdamW optimizer [21] for training, conducting experiments on a cluster of 8 NVIDIA A800 GPUs with a total batch size of 80. The learning rate is initialized as 1×10^{-4} and begins step decay starting at epoch 22, halving every two epochs. The model undergoes 30 epochs. More details can be referred to Appendix.

4.2. Leaderboard Performance

Figure 4 illustrates the detailed qualitative results for both marginal and joint predictions using our proposed method. ?? shows our qualitative marginal and joint prediction results. For additional qualitative results, please refer to Appendix.

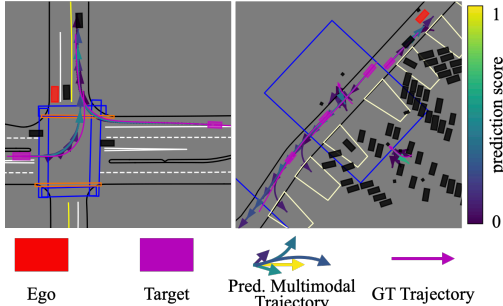


Figure 4. Visualization results for joint (left) and marginal (prediction) results.

Marginal Prediction Performance. Table 3 shows that our method achieves state-of-the-art (SOTA) performance on the Waymo 2024 motion prediction benchmark, outperforming all existing LiDAR-free approaches in the primary metric, Soft mAP, as well as in minADE and Overlap Rate. In the remaining metrics (mAP, minFDE, and Miss Rate), our method ranks second. Here, 'Ensemble' denotes the model-ensemble technique described in [26] for performance boosting, while 'Single' indicates evaluation with a single model.

Joint Prediction Performance. As presented in Table 4, even without any model-ensemble techniques [26], our single model achieves the best performance on the Waymo joint prediction leaderboard, surpassing the previous SOTA method [20] by 10.2% in both Soft mAP and mAP. Furthermore, our model attains the second-lowest Overlap Rate and the third-lowest Miss

Rate. These substantial improvements underscore the effectiveness of the IMPACT framework.

4.3. Behavioral Intention Prediction Performance

Table 1. Multimodal Behavioral Intention Prediction Performance.

Class	Precision	Top-1 Recall	F1-Score	Top-6 Accuracy	GT Data Ratio (%)
Ignored	0.99	0.97	0.98	0.99	89.12
Nearby	0.71	0.89	0.79	0.97	3.93
Overtaking	0.82	0.89	0.85	0.97	2.59
Yielding	0.86	0.96	0.90	0.97	4.32
All	0.97	0.97	0.97	0.987	100.00

Table 1 presents the results of multimodal behavioral intention prediction across four designated categories. Overall, the model demonstrates strong performance, with a F1-Score of 0.97, and a Top-6 accuracy of 0.987. In the dominant *Ignored* category, which comprises 89.12% of the dataset, our method attains particularly high accuracy (F1 = 0.98). Despite being underrepresented, the *Nearby*, *Overtaking*, and *Yielding* classes achieve F1-Scores between 0.79 and 0.90, showcasing the model's robustness in handling less frequent behaviors. These results underscore the model's effectiveness in accurately identifying and predicting diverse driver intentions, offering valuable insights for interpretable prediction models and informed downstream decision-making.

4.4. Vectorized Occupancy Prediction Performance

Table 2. Binary Classification Performance for top-1 mode Occupancy Prediction.

Class	Precision	Recall	F1-Score	GT Data Ratio (%)
Occupied	0.933	0.775	0.847	3.96
Unoccupied	0.991	0.998	0.994	96.04
All		0.989		100.00

Table 2 presents precision, recall, and F1-score for both classes, along with their data ratios in the validation set. The *occupied* class constitutes only 3.96% of samples, highlighting a strong imbalance. Despite this, the model achieves a high overall accuracy of 0.989. For the *occupied* class, precision (0.933) and recall (0.775) yield an F1-score of 0.847, indicating rare false positives—crucial for pruning irrelevant map polylines in trajectory prediction. The dominant *unoccupied* class achieves near-perfect precision (0.991), recall (0.998), and F1-score (0.994). These results demonstrate that our vectorized occupancy prediction effectively identifies critical map segments while minimizing false classification. More qualitative results are in Appendix.

4.5. Ablation Study

Different behavior modeling and map interaction mechanisms. Table 5 presents an ablation study evaluating various agent-pruning and map-pruning strategies on the validation set. The first row (All + Dynamic) queries all agents for the decoder while employing dynamic map selection as in MTR [26], serving as a baseline. Introducing agent selection via Braid Theory [20] (Row 2) enhances Soft mAP to 0.4602. Replacing Braid Theory with our two-class filtering—where Yielding, Overtaking, and

Table 3. Prediction on the test leaderboard of the motion prediction track of the Waymo Open Dataset Challenge. The first place is denoted by **bold**, the second place by underline, and the third place by *asterisk.

Method	Soft mAP \uparrow	mAP \uparrow	minADE \downarrow	minFDE \downarrow	Miss Rate \downarrow	Overlap Rate \downarrow
RMP-YOLO(Ensemble)[29]	0.4737	0.4531	0.5564	1.1188	0.1084	0.1259*
ModeSeq(Ensemble)[47]	<u>0.4737</u>	0.4665	0.5680	1.1766	0.1204	0.1275
BeTop[20]	0.4698	0.4587	0.5716	1.1668	0.1183	0.1272
MGTR[10]	0.4599	0.4505	0.5918	1.2135	0.1298	0.1275
EDA[19]	0.4596	0.4487	0.5718	1.1702	0.1169	0.1266
MTR++[27]	0.4410	0.4329	0.5906	1.1939	0.1298	0.1281
MTR[26]	0.4403	0.4249	0.5964	1.2039	0.1312	0.1274
HDGT[15]	0.3709	0.3577	0.5933	1.2055	0.1511	0.1557
DenseTNT[13]	-	0.3281	1.0387	1.5514	0.1573	0.1779
SceneTransformer[23]	-	0.2788	0.6117	1.2116	0.1564	0.1473
Ours (Ensemble)	0.4801	0.4598*	0.5563	<u>1.1295</u>	<u>0.1087</u>	<u>0.1258</u>
Ours (Single)	0.4721	<u>0.4609</u>	0.5641*	1.1540*	0.1143*	0.1255

Table 4. Joint Prediction on the test leaderboard of the interaction prediction track of the Waymo Open Dataset Challenge. The first place is denoted by **bold**, the second place by underline, and the third place by *asterisk.

Method	Soft mAP \uparrow	mAP \uparrow	minADE \downarrow	minFDE \downarrow	Miss Rate \downarrow	Overlap Rate \downarrow
BeTop-ens [20]	<u>0.2573</u>	<u>0.2511</u>	0.9779	2.2805	0.4376	0.1688*
BeTop [20]	0.2466*	0.2412*	0.9744	2.2744	0.4355	0.1696
MTR++ [27]	0.2368	0.2326	<u>0.8975</u>	<u>1.9509</u>	0.4143	0.1665
MTR [26]	0.2078	0.2037	0.9181*	2.0633	0.4411	0.1717
MotionDiffuser [16]	0.2047	0.1952	0.8642	1.9482	<u>0.4300</u>	0.2004
GameFormer [14]	0.1982	0.1923	0.9721	2.2146	0.4933	0.2022
BIFF [48]	0.1383	0.1229	0.9388	2.0443*	0.4620	0.2172
DenseTNT [13]	-	0.1647	1.1417	2.4904	0.5350	0.2309
M2I [31]	-	0.1239	1.3506	2.8325	0.5538	0.2757
SceneTransformer [23]	-	0.1192	0.9774	2.1892	0.4942	0.2067
Ours (Single)	0.2718	0.2659	0.9738	2.2734	0.4316*	<u>0.1684</u>

Nearby behaviors are treated as interactive while Ignore is considered non-interactive (Row 3)—further refines minADE to 0.5693 while maintaining a comparable Miss Rate. Notably, adopting our four-class YOIN approach (Row 4) elevates Soft mAP to 0.4728, demonstrating its ability to better capture nuanced interactions. Lastly, incorporating vectorized occupancy into YOIN (Row 5) further improves performance (Soft mAP = 0.4758), highlighting the benefit of explicit map filtering in isolating relevant polylines and refining trajectory predictions. These results validate the effectiveness of our integrated behavior modeling and map selection framework.

Number of selected agents and map polylines for behaviour-guided and occupancy-guided decoder.

On average, the model input contains 43.85 agents and 749.52 map polylines, meaning this selection reduces scene complexity by 45.2% and 74%, respectively, while preserving essential contextual cues. Beyond this threshold, redundant elements introduce noise, degrading generalization and increasing prediction uncertainty. This highlights the importance of selective context pruning to enhance trajectory forecasting performance.

Computational Efficiency and Parameter Analysis. We compare various agent-pruning and map-pruning strategies in Table 5 using the same encoder architecture. The first row (All + w/Dynamic) corresponds to a baseline that queries all agents and dynamically collect polylines, resulting in a model with 69.469 M parameters and a reported inference time of 14.67 ms under

a simplified setting. By contrast, our final approach (the last row in Table 5) combines YOIN-based agent pruning with vectorized occupancy-based pruning. This design lowers the parameter count to 48.944 M while reducing the average inference time of BeTOP[20] from 23.92 to 18.27 ms per scenario. The key to these efficiency gains lies in pruning irrelevant scene information—both agents and polylines—based on their semantic contributions, which in turn eliminates redundant computations. Notably, the approach retains or improves accuracy metrics such as Soft mAP, mAP, and minADE, underscoring that targeted context selection effectively balances computational efficiency with predictive performance.

Table 6. Performance gains from integrating proposed modules with existing approaches (Argoverse 1 & 2). **bFDE₆** is the main metric.

Method	bFDE ₆	mADE ₆	mFDE ₆	MR
SIMPL (AV2)	2.069	0.777	1.452	0.196
SIMPL+Ours (AV2)	1.921 (-7.1%)	0.743	1.387	0.178
HiVT (AV1)	1.662	0.661	0.969	0.092
HiVT+Ours (AV1)	1.556 (-6.4%)	0.599	0.932	0.087

Generalization Ability Study. To validate the cross-dataset and cross-paradigm generalization of our proposed symmetric dual filter, we conduct transfer experiments between the Waymo Open Dataset and Argoverse (AV1/AV2) using two distinct baselines: SIMPL (query-centric) and HiVT (agent-centric). As shown in Table 6, our approach achieves up to 7.1% (SIMPL on AV2)

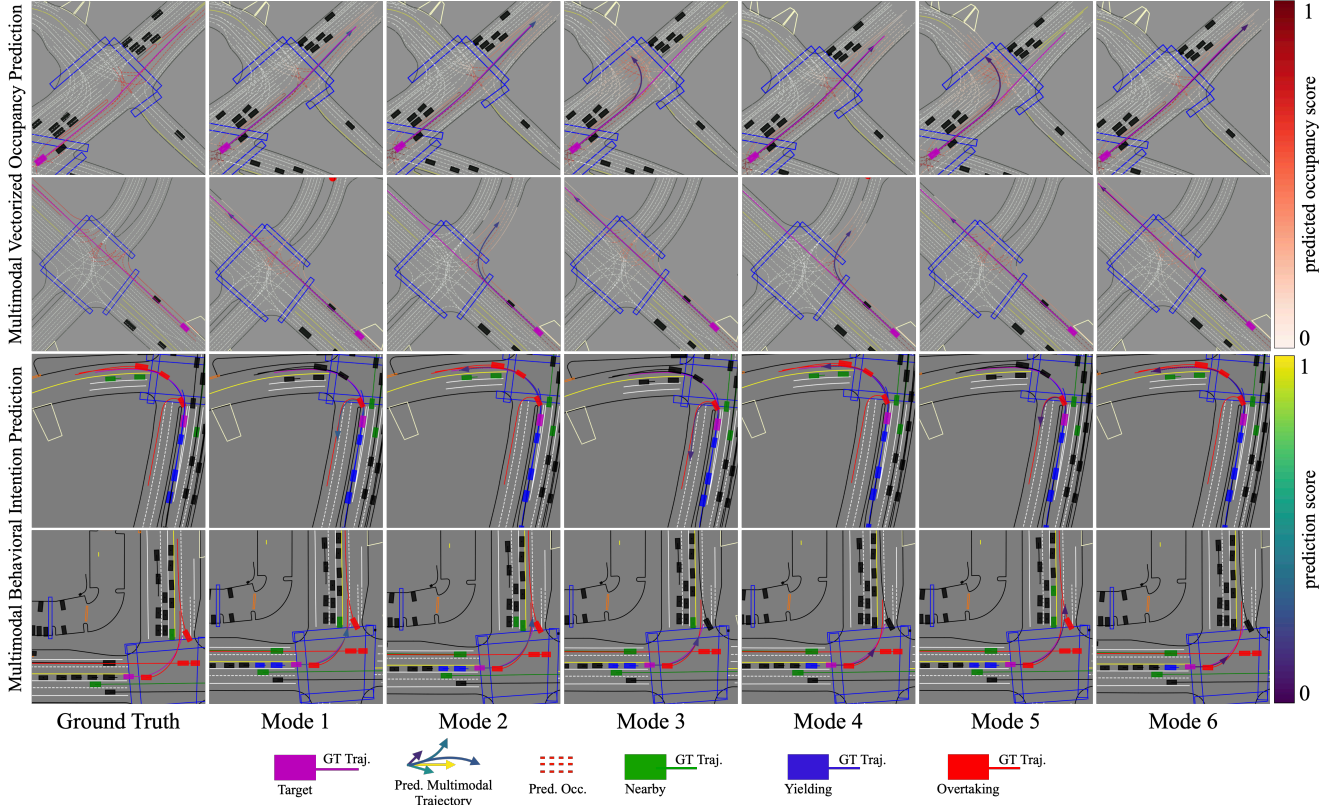


Figure 5. Visualization of Predicted Multimodal Occupancy and Intention Labels. In the top two rows, black agents represent other agents, while in the bottom two rows, they indicate ignored agents. Ground-truth trajectories are included for validation of predicted behaviors.

Table 5. Ablation study of different agent-pruning and map-pruning strategies on the validation set, using the same proposed encoder.

Agent			Map			Metrics						
All	w/Braid Theory[20]	w/Inter.	w/YOIN	w/Dynamic[26]	w/Vect. Occ.	Soft mAP	mAP	minADE	Miss Rate	Inference Time (ms/scenario)	Params (M)	
✓				✓		0.4582	0.4414	0.5718	0.1203	14.67	69.469	
	✓			✓		0.4602	0.4507	0.5745	0.1187	23.92	48.938	
		✓		✓		0.4663	0.4549	0.5693	0.1187	23.92	48.938	
			✓	✓		0.4728	0.4613	0.5680	0.1163	23.92	48.941	
			✓		✓	0.4758	0.4646	0.5652	0.1173	18.27	48.944	

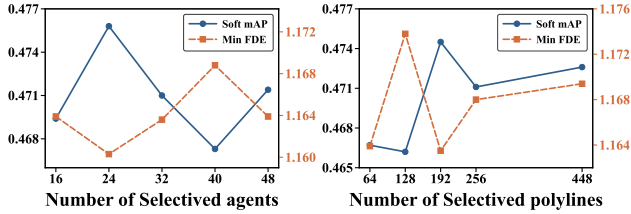


Figure 6. Results of varying numbers of selected agents and poly-lines for modeling on validation dataset.

and 6.4% (HiVT on AV1) improvements in bFDE₆. These results demonstrate our method’s versatility as a general enhancement framework, independent of specific network architectures.

5. Conclusion

In this paper, we present IMPACT, a novel and unified module that advances multimodal motion prediction through explicit modeling of behavioral intentions and dynamic context optimization.

The joint intention and motion modeling module eliminates redundancy and enables seamless information flow between behavioral semantic and motion dynamics, the experiments on both marginal and joint motion prediction challenges of large-scale WOMD show that our approach achieves state-of-the-art performance. The adaptive pruning decoder leverages intention and occupancy prediction priors to reduce computational complexity while preserving essential interaction cues. The automated labeling framework generates intention annotations across mainstream datasets and shows great scalable performance.

Limitations and Future work. Our pruning mechanism prioritizes instantaneous interactions, potentially overlooking evolving multi-agent gaming dynamics. Extending the framework with temporal graph networks or recursive reasoning could enhance long-horizon interaction modeling. We plan to incorporate this idea into both the latest end-to-end and traditional planning frameworks, particularly to address the challenge of determining which agent to predict and which polyline to focus on.

References

- [1] Argoverse. Argoverse motion forecasting competition, . Accessed: 2024-08-31. 2
- [2] Argoverse. Argoverse 2: Motion forecasting competition, . Accessed: 2024-08-31. 2
- [3] Prarthana Bhattacharyya, Chengjie Huang, and Krzysztof Czarnecki. Ssl-lanes: Self-supervised learning for motion forecasting in autonomous driving, 2022. 3
- [4] Yuning Chai, Benjamin Sapp, Mayank Bansal, and Dragomir Anguelov. Multipath: Multiple probabilistic anchor trajectory hypotheses for behavior prediction, 2019. 2
- [5] Jie Cheng, Xiaodong Mei, and Ming Liu. Forecast-MAE: Self-supervised pre-training for motion forecasting with masked autoencoders. *Proceedings of the IEEE/CVF International Conference on Computer Vision*, 2023. 3
- [6] Sehwan Choi, Jungho Kim, Junyong Yun, and Jun Won Choi. R-pred: Two-stage motion prediction via tube-query attention-based trajectory refinement, 2023. 2, 3
- [7] Nachiket Deo, Eric M. Wolff, and Oscar Beijbom. Multimodal trajectory prediction conditioned on lane-graph traversals, 2021. 2
- [8] Jianwu Fang, Fan Wang, Jianru Xue, and Tat seng Chua. Behavioral intention prediction in driving scenes: A survey, 2023. 3
- [9] Chen Feng, Hangning Zhou, Huadong Lin, Zhigang Zhang, Ziyao Xu, Chi Zhang, Boyu Zhou, and Shaojie Shen. Mac-former: Map-agent coupled transformer for real-time and robust trajectory prediction. *IEEE Robotics and Automation Letters*, 8(10):6795–6802, 2023. 4
- [10] Yiqian Gan, Hao Xiao, Yizhe Zhao, Ethan Zhang, Zhe Huang, Xin Ye, and Lingting Ge. Mgrtr: Multi-granular transformer for motion prediction with lidar, 2024. 3, 7
- [11] Jiyang Gao, Chen Sun, Hang Zhao, Yi Shen, Dragomir Anguelov, Congcong Li, and Cordelia Schmid. Vectornet: Encoding hd maps and agent dynamics from vectorized representation, 2020. 2
- [12] Thomas Gilles, Stefano Sabatini, Dzmitry Tsishkou, Bogdan Stanculescu, and Fabien Moutarde. Home: Heatmap output for future motion estimation, 2021. 2
- [13] Junru Gu, Chen Sun, and Hang Zhao. Densetnt: End-to-end trajectory prediction from dense goal sets, 2021. 2, 7
- [14] Zhiyu Huang, Haochen Liu, and Chen Lv. Gameformer: Game-theoretic modeling and learning of transformer-based interactive prediction and planning for autonomous driving, 2023. 7
- [15] Xiaosong Jia, Penghao Wu, Li Chen, Yu Liu, Hongyang Li, and Junchi Yan. Hdgt: Heterogeneous driving graph transformer for multi-agent trajectory prediction via scene encoding. *IEEE Transactions on Pattern Analysis and Machine Intelligence*, 45(11):13860–13875, 2023. 2, 7
- [16] Chiyu Max Jiang, Andre Cornman, Cheolho Park, Ben Sapp, Yin Zhou, and Dragomir Anguelov. Motiiondiffuser: Controllable multi-agent motion prediction using diffusion, 2023. 7
- [17] Zhiqian Lan, Yuxuan Jiang, Yao Mu, Chen Chen, and Shengbo Eben Li. Sept: Towards efficient scene representation learning for motion prediction, 2023. 2, 3
- [18] Longzhong Lin, Xuewu Lin, Tianwei Lin, Lichao Huang, Rong Xiong, and Yue Wang. Eda: Evolving and distinct anchors for multimodal motion prediction, 2023. 3
- [19] Longzhong Lin, Xuewu Lin, Tianwei Lin, Lichao Huang, Rong Xiong, and Yue Wang. Eda: Evolving and distinct anchors for multimodal motion prediction. In *Proceedings of the AAAI Conference on Artificial Intelligence*, pages 3432–3440, 2024. 2, 7
- [20] Haochen Liu, Li Chen, Yu Qiao, Chen Lv, and Hongyang Li. Reasoning multi-agent behavioral topology for interactive autonomous driving, 2024. 2, 3, 6, 7, 8
- [21] Ilya Loshchilov and Frank Hutter. Decoupled weight decay regularization, 2019. 6
- [22] Norman Mu, Jingwei Ji, Zhenpei Yang, Nate Harada, Hao-tian Tang, Kan Chen, Charles R. Qi, Runzhou Ge, Kratharth Goel, Zoey Yang, Scott Ettinger, Rami Al-Rfou, Dragomir Anguelov, and Yin Zhou. Most: Multi-modality scene tokenization for motion prediction, 2024. 3
- [23] Jiquan Ngiam, Benjamin Caine, Vijay Vasudevan, Zhengdong Zhang, Hao-Tien Lewis Chiang, Jeffrey Ling, Rebecca Roelofs, Alex Bewley, Chenxi Liu, Ashish Venugopal, David Weiss, Ben Sapp, Zhifeng Chen, and Jonathon Shlens. Scene transformer: A unified architecture for predicting multiple agent trajectories, 2022. 7
- [24] Tung Phan-Minh, Elena Corina Grigore, Freddy A. Boulton, Oscar Beijbom, and Eric M. Wolff. Covernet: Multimodal behavior prediction using trajectory sets, 2020. 2
- [25] Chen Shi, Shaoshuai Shi, and Li Jiang. Mtr v3: 1st place solution for 2024 waymo open dataset challenge - motion prediction. Technical report, The Chinese University of Hong Kong (Shenzhen) and DiDi Global, 2024. 2
- [26] Shaoshuai Shi, Li Jiang, Dengxin Dai, and Bernt Schiele. Motion transformer with global intention localization and local movement refinement, 2023. 2, 3, 5, 6, 7, 8
- [27] Shaoshuai Shi, Li Jiang, Dengxin Dai, and Bernt Schiele. Mtr++: Multi-agent motion prediction with symmetric scene modeling and guided intention querying, 2024. 1, 2, 3, 7
- [28] Nan Song, Bozhou Zhang, Xiatian Zhu, and Li Zhang. Motion forecasting in continuous driving, 2024. 3
- [29] Jiawei Sun, Jiahui Li, Tingchen Liu, Chengran Yuan, Shuo Sun, Zefan Huang, Anthony Wong, Keng Peng Tee, and Marcelo H. Ang Jr. Rmp-yolo: A robust motion predictor for partially observable scenarios even if you only look once, 2024. 2, 3, 4, 7
- [30] Jiawei Sun, Chengran Yuan, Shuo Sun, Shanze Wang, Yuhang Han, Shuailei Ma, Zefan Huang, Anthony Wong, Keng Peng Tee, and Marcelo H. Ang Jr. Controlmtr: Control-guided motion transformer with scene-compliant intention points for feasible motion prediction, 2024. 3
- [31] Qiao Sun, Xin Huang, Junru Gu, Brian C. Williams, and Hang Zhao. M2i: From factored marginal trajectory prediction to interactive prediction, 2022. 7
- [32] Xiaolong Tang, Meina Kan, Shiguang Shan, Zhilong Ji, Jinfeng Bai, and Xilin Chen. Hpnet: Dynamic trajectory forecasting with historical prediction attention, 2024. 3
- [33] Balakrishnan Varadarajan, Ahmed Hefny, Avikalp Srivastava, Khaled S. Refaat, Nigamaa Nayakanti, Andre Cornman, Kan Chen, Bertrand Douillard, Chi Pang Lam,

- Dragomir Anguelov, and Benjamin Sapp. Multipath++: Efficient information fusion and trajectory aggregation for behavior prediction, 2021. [2](#), [4](#)
- [34] Ashish Vaswani, Noam Shazeer, Niki Parmar, Jakob Uszkoreit, Llion Jones, Aidan N. Gomez, Lukasz Kaiser, and Illia Polosukhin. Attention is all you need, 2023. [3](#)
- [35] Mingkun Wang, Xiaoguang Ren, Ruochun Jin, Minglong Li, Xiaochuan Zhang, Changqian Yu, Mingxu Wang, and Wenjing Yang. FutureNet-LoF: Joint trajectory prediction and lane occupancy field prediction with future context encoding, 2024. [2](#)
- [36] Mingkun Wang, Xiaoguang Ren, Ruochun Jin, Minglong Li, Xiaochuan Zhang, Changqian Yu, Mingxu Wang, and Wenjing Yang. FutureNet-LoF: Joint trajectory prediction and lane occupancy field prediction with future context encoding, 2024. [1](#)
- [37] Sheng Wang, Yingbing Chen, Jie Cheng, Xiaodong Mei, Ren Xin, Yongkang Song, and Ming Liu. Improving autonomous driving safety with pop: A framework for accurate partially observed trajectory predictions. In *2024 IEEE International Conference on Robotics and Automation (ICRA)*, pages 14450–14456. IEEE, 2024. [3](#)
- [38] Waymo. Waymo open dataset: Motion prediction challenge. Accessed: 2024-08-31. [2](#), [6](#)
- [39] Bozhou Zhang, Nan Song, and Li Zhang. Demo: Decoupling motion forecasting into directional intentions and dynamic states, 2024. [3](#)
- [40] Lu Zhang, Peiliang Li, Sikang Liu, and Shaojie Shen. Simpl: A simple and efficient multi-agent motion prediction baseline for autonomous driving, 2024. [2](#)
- [41] Hang Zhao, Jiyang Gao, Tian Lan, Chen Sun, Benjamin Sapp, Balakrishnan Varadarajan, Yue Shen, Yi Shen, Yuning Chai, Cordelia Schmid, Congcong Li, and Dragomir Anguelov. Tnt: Target-driven trajectory prediction, 2020. [2](#)
- [42] Xiaoji Zheng, Lixiu Wu, Zhijie Yan, Yuanrong Tang, Hao Zhao, Chen Zhong, Bokui Chen, and Jiangtao Gong. Large language models powered context-aware motion prediction, 2024. [3](#)
- [43] Yang Zhou, Hao Shao, Letian Wang, Steven L. Waslander, Hongsheng Li, and Yu Liu. Smartrefine: A scenario-adaptive refinement framework for efficient motion prediction, 2024. [2](#)
- [44] Zikang Zhou, Luyao Ye, Jianping Wang, Kui Wu, and Kejie Lu. Hivt: Hierarchical vector transformer for multi-agent motion prediction. In *2022 IEEE/CVF Conference on Computer Vision and Pattern Recognition (CVPR)*, pages 8813–8823, 2022. [2](#)
- [45] Zikang Zhou, Jianping Wang, Yung-Hui Li, and Yu-Kai Huang. Query-centric trajectory prediction. In *Proceedings of the IEEE/CVF Conference on Computer Vision and Pattern Recognition (CVPR)*, pages 17863–17873, 2023. [1](#), [2](#)
- [46] Zikang Zhou, Zihao Wen, Jianping Wang, Yung-Hui Li, and Yu-Kai Huang. Qcnext: A next-generation framework for joint multi-agent trajectory prediction, 2023. [2](#)
- [47] Zikang Zhou, Jianping Wang, Yung-Hui Li, and Yu-Kai Huang. Modeseq: Technical report for 2024 waymo open motion dataset challenge - motion prediction. Technical report, City University of Hong Kong, Hon Hai Research Institute, Carnegie Mellon University, 2024. [1](#), [3](#), [7](#)
- [48] Yiyao Zhu, Di Luan, and Shaojie Shen. Biff: Bi-level future fusion with polyline-based coordinate for interactive trajectory prediction, 2023. [7](#)